Int. J. Electrochem. Sci., 8 **(2013)** 5515 - 5528

International Journal of
ELECTROCHEMICAL
SCIENCE
www.electrochemsci.org

Tribological and Corrosion Characterization of Al/(Stellite-6+Zirconium) Laser Alloyed Composites

T. G. Rambau[1], *A. P. I. Popoola*[*,1], *C.A. Loto*[1], *T. Mathebula*[1,2] *and M. Theron*[2]

[1]Department of Chemical and Metallurgical Engineering, Faculty of Engineering and the Built Environment, Tshwane University of Technology, Pretoria, X680 South Africa 0001.
[2]Center for Scientific and Industrial Research – National Laser Centre, P.O. Box 395, BLD 46F, Pretoria, South Africa, 0001.
[*]E-mail: popoolaapi@tut.ac.za;

Received: 29 January 2013 / *Accepted:* 15 March 2013 / *Published:* 1 April 2013

Excellent display of surface dependent properties by metals and alloys are pre-requisite for efficient engineering operations in the industry. In this work, AA1200 laser alloyed surface was investigated for its hardness, wear and corrosion behaviour at different laser processing conditions. Stellite-6 and zirconium powders were used as ceramic and metallic reinforcement materials respectively; these were chosen in order that all required surface properties are improved. A continuous wave Rofin Sinar Nd:YAG laser emitting 1.064 μm wavelength was utilized for the fabrication process. The microstructures of the developed composites were characterized by optical (OM) and scanning electron microscopes (SEM/EDS). Equally, x-ray diffractometer (XRD) was used to identify the phases present. The addition of alloying elements increased the hardness, wear and corrosion resistances. The improvement of these properties was attributed to the formation of new phases and the microstructures evolved on the surface of the laser alloyed aluminium AA1200.

Keywords: Laser surface alloying, grain refinement, microstructure

1. INTRODUCTION

Aluminium alloys have found intensive use in most industries because of the numerous attractive properties they possess [1-17]. These alloys are increasingly used as structural materials in aerospace and automobile industries because of their light weight coupled with their excellent mechanical strength. The availability of aluminium minerals in almost all countries in the world makes it a relatively cheap metal; and the high strength to weight ratio displayed has indeed increased the usage of these alloys round about the world [3-17]. Other desirable properties that these alloys exhibit

are: good workability and excellent thermal and electrical conductivities. However, aluminium alloys still perform poorly in certain service conditions requiring high hardness and wear resistance and also in aggressive corrosion environments, despite all the attractive properties. All the properties mentioned above are regarded as surface dependent properties [11-12]. The high affinity of aluminium alloys for oxygen lead to the formation of thin oxide film of Al_2O_3 on its surface when exposed to the atmosphere. However, aluminium degrades when exposed to aggressive environments for example in chloride medium, the surface film on aluminium is seriously attacked hence corrosion degradation reactions proceeds. These alloys possess very low hardness which is because of the weak interatomic bonds they have. The wear resistance of some materials is directly related to their hardness properties, there is however very little correlation between hardness and corrosion behavior of materials.

Hence, methods for surface modification such as laser surface alloying (LSA) becomes a novel tool for improving these drawbacks. Laser surface alloying (LSA) has been demonstrated to be a useful method for improving the surface dependent properties of aluminium by a number of authors [1-13] and improvements in wear resistance is possible [14]. Laser surface alloying is a sophisticated materials processing technique which involves the scanning of the laser beam across the material's surface creating a pool of the molten substrate. This is followed by immediate deposition of reinforcement powder particles thereby forming an alloy with composition and phases/microstructure different from the substrate material. The efficiency of the process depends to a large extent on the correct application of processing parameters. Important parameters such as laser power, scan speed and powder feed rate needs to be well optimized. This process is an heterogeneous process, where different alloy compositions and a range of novel microstructures and phases are developed leading to enhanced surface properties of the substrate [15, 16].

Quite a number of authors have reported on the improvement of chemical and mechanical properties by using laser surface technique:

[5] reported on the laser surface alloying of aluminium AA1200. Ni, Ti and SiC powders were used as reinforcement material for alloying. The reaction between Al and the Ni resulted in the formation of in-situ intermetallic phases such as Al_3Ni and Al_3Ni_2 and Al_3Ti. SiC particles reacted with Al or Ti to form Al_4C_3, Al_4SiC_4, TiC or Ti_3SiC_2 and Ti_5Si_3 phases. The increase in hardness was due to the formation of metal matrix composites and intermetallic compounds.

Laser surface alloying AA6061 with TiNi to improve the wear resistance was done by [9]. The intermetallic compounds including Ni-Al and Ti-Al were formed by the laser surface alloying technique. A continuous Nd: YAG laser was used in an argon atmosphere. XRD results were used to confirm the new phases that were formed $TiAl_3$ and Ni_3Al. An increase in hardness from below 100 HV of the untreated surface to more than 350 HV of the alloyed layer. The increase in hardness led to the increase in the wear resistance of the modified layer which is about 5.5 times that of the substrate.

[17] reported the wear improvement of aluminium alloyed with W+Co+NiCr. A 5 kW continuous wave Nd: YAG laser was used with an output power ranging from 3 to 3.5 kW and scan speed from 0.012 m/s to 0.04 m/s. An investigation on the effect of laser power and scan speed on the microstructure, phases and composition and hence the resultant properties (wear and corrosion resistance) were done. There was an improvement on the microhardness of the alloyed zone to a value of 650 VHN compared to 22 VHN of as-received aluminium sample. The improvement in hardness

was achieved by the formation of new phases and intermetallic compounds formed such as WC, W_2C, Al_4C_3, Al_9Co_2, Al_3Ni, $Cr_{23}C_6$, and Co_6W_6C developed. Improvement in wear resistance of the alloyed sample was achieved when fretting wear testing method was used.

[18] investigated the microstructure and wear resistance of laser alloyed Al-Mg-Si with Co powder. A continuous wave CO_2 laser was used. There was formation of Al_9Co_2 particles at the alloyed surface region and $Al_{13}Co_4$ particles distributed at the bottom region of the alloyed surface. The hardness increased three times more that of aluminium sample. The increase in hardness resulted in an increase in sliding wear performance and a lower friction co-efficient and wear rate.

Attempts will be made in this present work to improve the surface properties of AA 1200 using LSA technique. A combination of two reinforcement powders will be used to form unique properties. Stellite-6 and zirconium will be mixed at a ratio of 50:50. Chemically, zirconium is highly reactive in air or aqueous media; which aid the formation of oxide film thereby protecting it against corrosion attack. Zirconium is stable in acid and caustic media. Zirconium alloy is similar to titanium in that it is considered a reactive metal reason being that it displays a high affinity for oxygen [19]. Stellite-6 is a cobalt-chromium alloys designed for wear resistance. It contains tungsten or molybdenum and a small amount of carbon can also be present. The properties of this alloy are that, it is non-magnetic and slightly corrosion resistant. Retains its hardness at high temperature and resists oxidation upto 1095°C. This compound of cobalt is especially good for obtaining high wear resistance.

The present study investigates the influence of reinforcement additions on the properties and microstructure of laser surface alloyed AA1200 metal matrix composite, the aim is develop materials with excellent surface properties (hardness, wear and corrosion resistances).

2. EXPERIMENTAL PROCEDURE

2.1. Laser surface alloying

AA1200 is the substrate material, the chemical composition of this alloy can be found in Table 3. A 4.4 kW Rofin Sinar Nd: YAG laser was used for laser surface alloying of AA1200 aluminium alloy with stellite-6 and zirconium reinforcement powders. A KUKA robotic arm was used for the positioning of the laser processing head. AA1200 was cut to with dimensions of 100 x 100 x 6 mm. Oxidation was prevented by the use of argon as an inert gas. Stellite-6 and zirconium powder particles were mixed in a ratio of 50:50. The powder particles were transported to the substrate through the off-axis nozzle from the powder feed hopper. Sandblasting of aluminium substrate was done in order to increase its absorptivity thereby reducing its reflectivity. The laser surface alloying was done by scanning the laser beam on aluminium substrate thus depositing the powder particles inside the melt pool generated by the beam. Optimization of the alloying process was carried out. The laser power and scan speed were varied while other parameters such as beam diameter, powder flow and shielding gas flow rate were kept constant (Table 2). An overlap rate of 75% was adopted. Table 1 shows the processing data for the composites developed.

Table 1. Laser surface alloying parameters at 75% overlap

Sample No.	Sample	Power	Scan speed	Beam diameter	Powder flow	Shielding gas	Shielding gas flow
1	Al-Stellite-Zr (ASZ-1)	4 kW	1.0 m/min	3 mm	3 g/min	Argon	2 l/min
2	Al-Stellite-Zr (ASZ-2)	4 kW	1.2 m/min	3 mm	3 g/min	Argon	2 l/min

2.2. Metallurgical preparation

The samples were prepared metallographically by cross sectioning with a corundum cut-off wheel and hot mounting with heat and pressure mounting press. Grinding was done with SiC papers at 320-1200 grit size with water as a lubricant. Polishing was done using different cloths of 9, 3 and 0.04 μm with relevant lubricants. A flat mirror-like surface is required for good surface analysis. After metallurgical preparation, the alloyed samples were observed under light optical microscope and scanning electron microscope for the microstructure and compositional analyses. Further surface analysis done was XRD for the identification of the new phases formed by the reaction between the powder particles and the substrate in the melt pool. The X' Pert Pro diffractometer consisted of Cu Kα radiation that was set at 45 kV and 40 mA. Scanning was done in a range between 5° and 90° two theta (2θ) with a step size of 0.02 degree.

2.3. Microhardness test

The substrate was tested using the Vicker's micro-hardness tester with a diamond indenter. The load of 100 g, spacing of 100-150 μm and a dwelling time of 10 seconds were used as parameters for material testing. The alloyed materials were tested for hardness along the interface of alloyed zone, a through thickness indentation profile.

2.4. Electrochemical test

Electrochemical test was carried out by using Potentiostatic Autolab incorporated with Nova 1.8 version software. The samples were cold mounted with a resin epoxy and ground down to 600 μm grit size. A 3.65% NaCl solution was used as a medium for corrosion test which was prepared by the use of grade reagents and distilled water. The reference electrode of Ag/AgCl with platinum rod as a counter electrode and working electrode as the sample were all immersed in a solution. Linear polarization was done by scanning from -1.0 to 0.5 V potential for duration of 3600 seconds (1 h). All the potentials reported were versus the SCE potentials.

2.5. Wear test

The three body abrasive wear test was used to measure the resistance of laser alloyed material against wear and compared with that of the substrate. The ASTM-G65 was used as a standard test procedure for wear. Three parameters were varied. The silica sand was used as an abrasive with a flow rate of 6.9 g/s and its particle size distribution ranged between 300-600 µm. The sample was subjected to a load of 2.5 kg with a rotating speed of 200 rpm. The dimension of the sample that was placed in the machine was 65 x 25 mm. Test duration for each sample is 30 minutes. After the procedure, each sample was weighed to determine its mass loss.

3. RESULTS AND DISCUSSION

3.1. Materials characterization

Figure 1 (a) shows the SEM image of the stellite-6 powder used for the processing of laser alloying. The morphology of this powder shows it is roundish in shape; it is also very heavy alloy of cobalt. EDS of this alloy can be seen in Figure 1 (b), while its chemical composition is shown in Table 2.

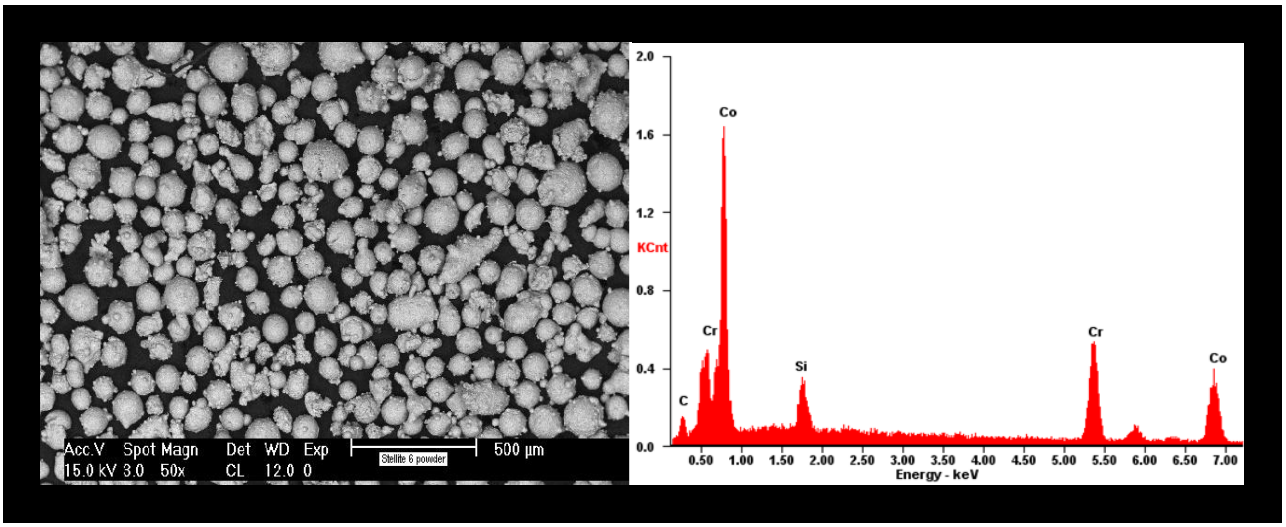

Figure 1. (a) SEM and (b) EDS spectra of stellite-6 powder

The chemical composition along with the EDS analysis confirms that it contains a high content of cobalt and chromium metals. The presence of these two metals in the matrix of aluminium increased the corrosion resistance of aluminium. The combined weight percentage of the two elements is approximately 85%. X-ray diffractograph analysis of the powder shows the presence of these phases: Ni, Cr, Ni_2Si, $CFe_{2.5}$ and $Co_{0.72}Fe_{0.28}$.

Table 2. Chemical composition of stellite-6 (wt.%)

Element	Fe	Mn	Cr	Ni	Co	Nb	W
Stellite-6 (wt.%)	2.26	0.28	26.48	3.26	59.55	0.068	8.095

Figure 2 (a) presents the SEM image of zirconium powder used as reinforcement. The morphology of Zr powder is irregular and flat. The powder used is pure. XRD spectrum as seen in Figure 2 (b) confirmed the phases present to be only zirconium.

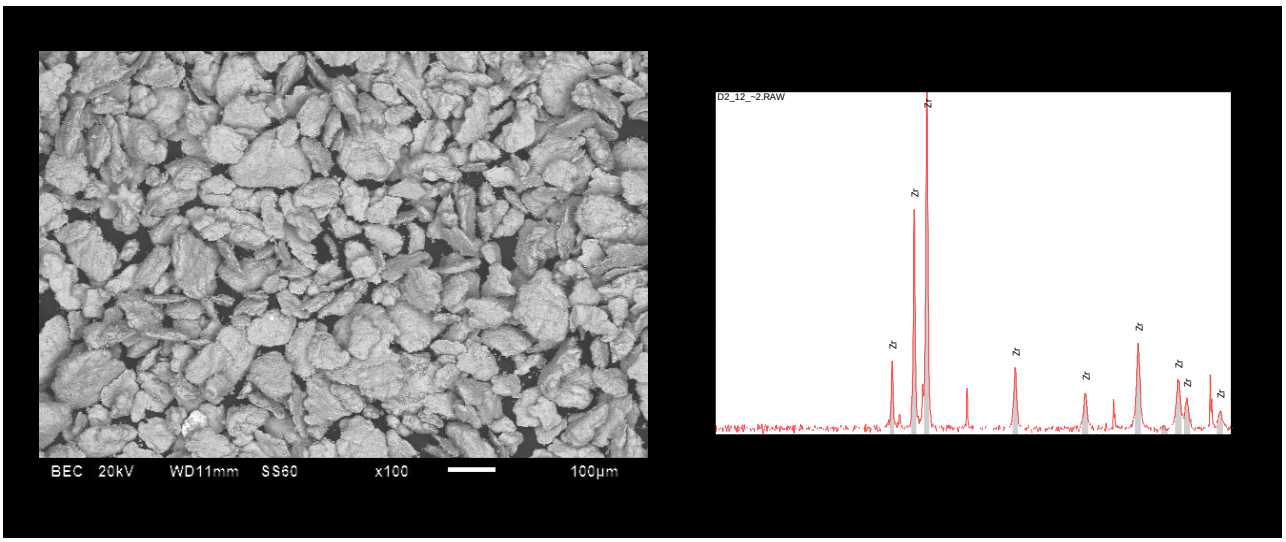

Figure 2. (a) SEM and (b) X-ray spectra of zirconium powder

The chemical composition of the aluminium AA1200 substrate material can be seen in Table 3.

Table 3. Chemical composition of AA 1200 aluminium

Elements	Cu	Si	Fe	Al
Chemical composition (wt %)	0.12	0.13	0.59	Balance

The SEM and EDS spectra of the substrate are presented in Figure 3 where the morphology can be seen. The white phases consist of Fe whereas the dark greyish phase is the Al-matrix.

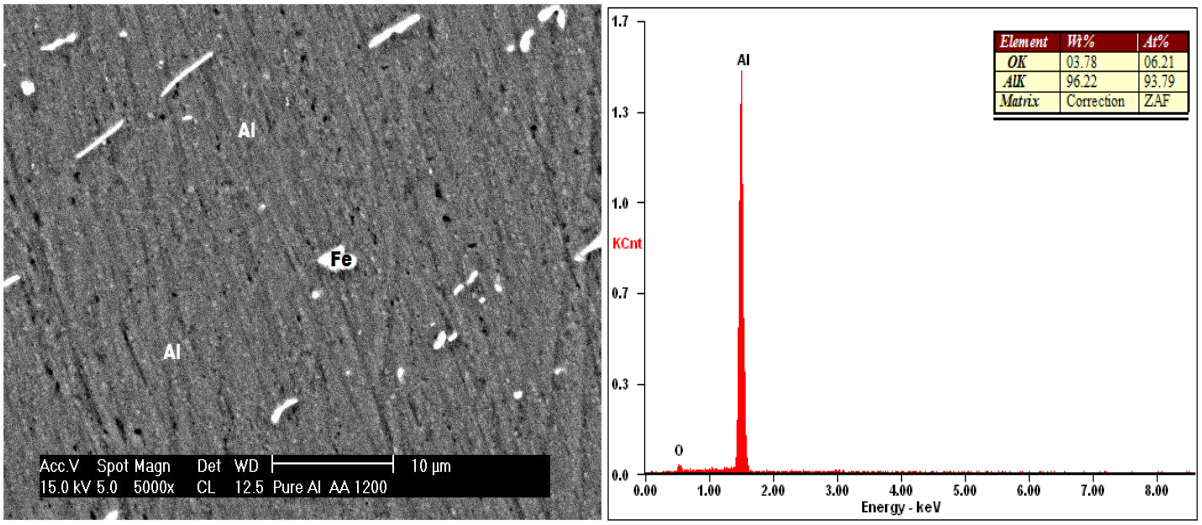

Figure 3. SEM and EDS spectra of AA1200

Using the Energy Dispersive Spectroscopy (EDS) analysis, the elemental composition of AA1200 alloy was confirmed. The XRD analysis was also carried to identify phases present in the Al; peaks of Al and Fe were identified, an evidence of the purity of the substrate.

3.2. Microstructural characterization of alloyed samples

Figure 4 is the SEM micrograph of the alloyed sample (ASZ 2). The surface morphology of the newly formed laser alloyed aluminium matrix is shown below. The kind of microstructure that resulted is needle-like microstructures which were uniformly dispersed across the Al-matrix.

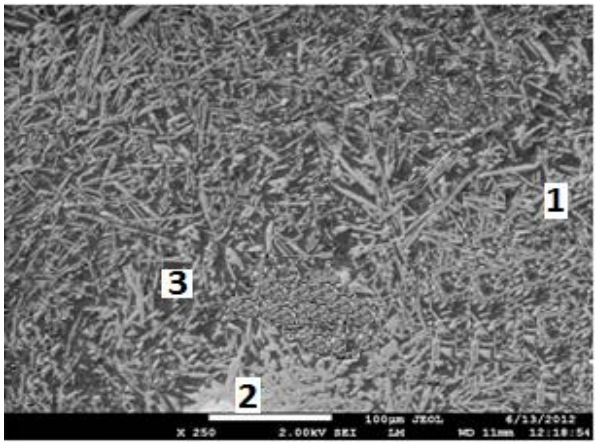

Figure 4. SEM image of alloyed sample ASZ-2

There was some small amount of unmelted powder particles that were evidence within the newly formed laser alloyed matrix. There were grey micro-platelets microstructures which were

uniformly distributed along the matrix of the substrate. The grey platelet indicated by area 1 is aluminium which is present in high percentage with zirconium, Co and Cr in small percentages. Al-Zr phase is present in high percentage in area 2 than other elements. Heavy metals appear bright while light metals appear dark in colour. The area indicated by 3 is aluminium, the base metal and it appears dark.

The optical micrograph of the alloyed ASZ samples can also be seen in Figure 5.

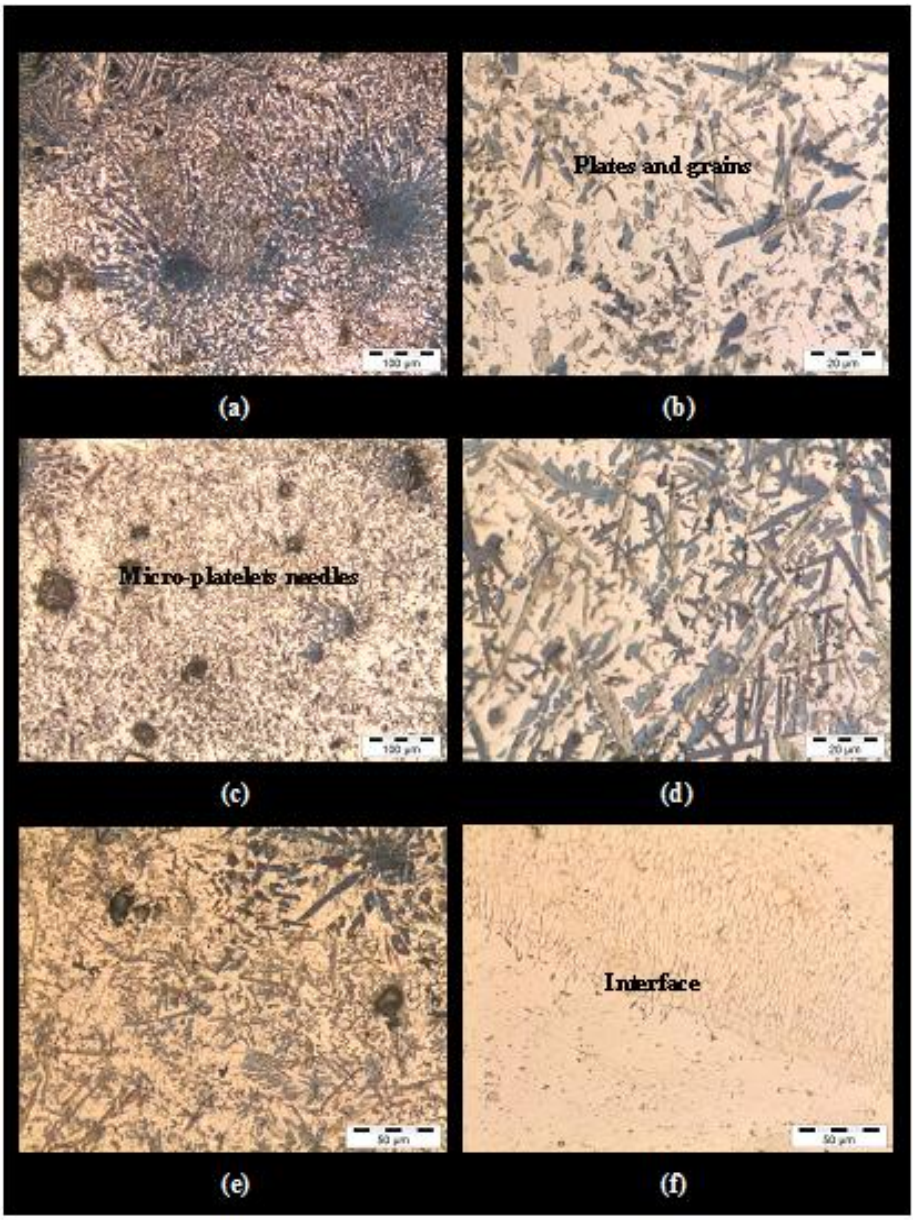

Figure 5. Optical micrograph of alloyed sample: (a)-(b) Sample ASZ-1, (c)-(d) Sample ASZ-2 and (f) typical interface of alloyed layer.

From the optical micrographs, it can be seen that the microstructures evolved for all the samples revealed platelets needle-like microstructure. Sample ASZ-2 (f) reveals the interface of the alloyed layer and the substrate which shows good metallurgical bonding.

The XRD analysis of ASZ sample shows the formation of new phases in Al matrix as seen in Figure 6. Primary phases that were identified include Al_3Co and Al_3Zr and α-Al.

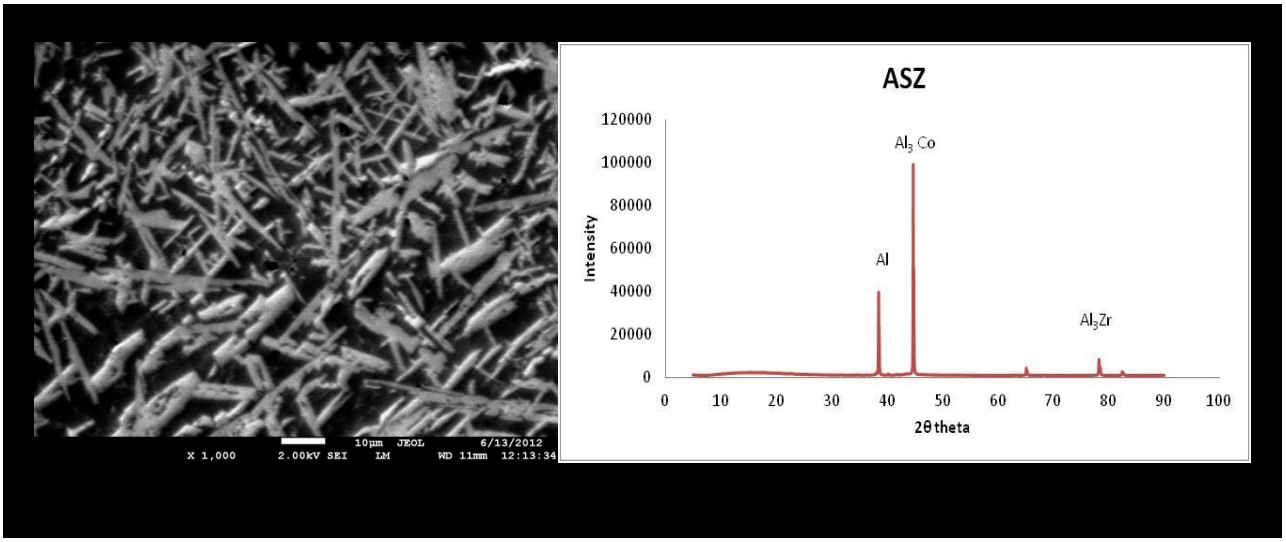

Figure 6. (a) SEM and (b) XRD of ASZ-2 alloyed sample

3.3. Microhardness characterization

Table 4 presents the microhardness values of the alloyed samples.

Table 4. Average microhardness data

Sample no.	Admixtured composition	Scan speed (m/min)	Power (kW)	Average hardness (HV0.1)
ASZ-1	Al-Stellite-Zr	1.0	4	212
ASZ-2	Al-Stellite-Zr	1.2	4	160

The micro-hardness value of AA1200 substrate was measured to be ± 24 HV. There was an increase in micro-hardness of the laser alloyed matrix compared to that of pure aluminium matrix. The hardness increased to about 5-9 times that of the substrate. The average hardness values were calculated by measuring 15 indents along the interface of the laser alloyed matrix (Table 4). There was a linear decrease in average hardness from sample ASZ-1 to sample ASZ-2 (Figure 7). The decrease in average hardness was caused by the increase in the scan speed. As the scan speed increases the average hardness of the samples reduces. The scan speed is inversely proportional to the energy input; which then means that at lower speeds the energy will be high and this will permit a wider melt pool and inevitably lead to more injected powder into the melt pool as such the alloyed zone will have higher powder fraction than samples fabricated at higher speeds.

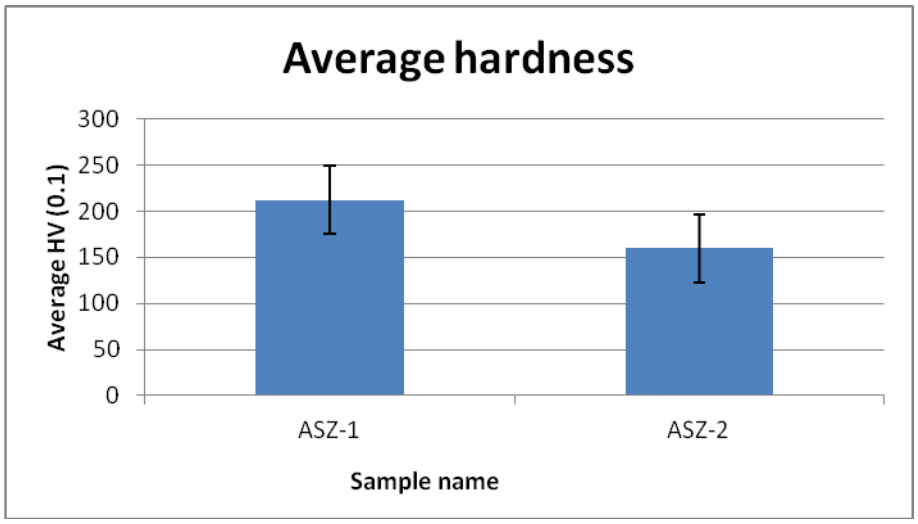

Figure 7. Average microhardness of laser alloyed sample

3.4. Wear characterization

Table 5 below revealed the three body abrasive wear test results. The initial mass and the final mass of the samples were recorded together with the difference between them. The wear rate was calculated by dividing the mass loss with the time taken for abrasion.

Table 5. Wear test data

Sample number	Initial mass (g)	Final mass (g)	Mass loss (g)	Time (min)	Wear rate (g/min)
ASZ-1	12.761	12.729	0.032	30	0.001067
ASZ-2	11.376	11.35	0.026	30	0.000867
As-Received	14.265	14.171	0.094	30	0.003133

The results showed an exponential increase in wear rate from sample ASZ-1 to as-received sample (Figure 8). As-received sample showed a higher wear rate as compared to laser alloyed samples. The rate in which the material wears when subjected to abrasive silica sand is minimal for sample ASZ-2; this showed that there was resistance of alloyed material to wear. The resistance of the material to wear was caused by the formation of new phases as a result of laser surface alloying with a combination of stellite-6 and zirconium powders.

The worn surface of the AA 1200 shows signs of wear debris, pits, shallow grooves and severe plastic deformation pointing out that the wear mechanism is adhesion and abrasive wear. Plastic deformation is very minimal on the worn surface of the alloyed materials; however some debris and grooves were evident on the worn surfaces. This indicates that the wear mechanisms of the coatings are mainly abrasive and adhesion wears.

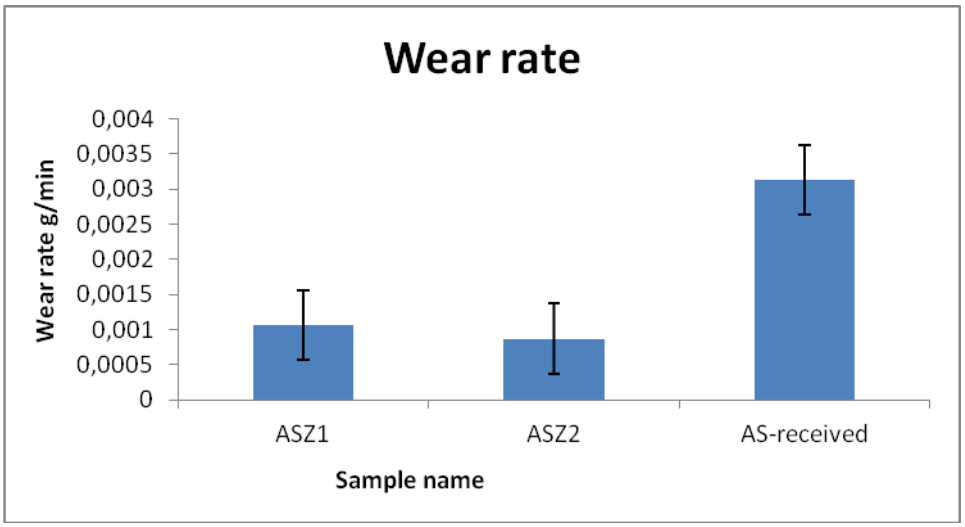

Figure 8. Wear rate of samples

The alloyed materials revealed mild abrasive wear while the substrate exhibits severe wear. Figure 8 show that the alloyed layers exhibited higher wear resistance than the substrate as a result of the formation of the new phases. ASZ-2 sample displayed better wear resistance than ASZ-1 sample which was attributed to the fact that reinforcement materials are better dispersed in the Al-matrix, eliminating microsegregation thus enhancing uniform resistance to deformation.

3.5. Corrosion characterization

Table 6. Polarization data for the alloyed and as-received samples

Samples	E_{corr} (V)	j_{corr} (A/cm^2)	i_{corr} (A)	R_p (Ω)	CR (mm/yr)
AA 1200	-1.036	2.3×10^{-6}	1.5×10^{-6}	2.6×10^{3}	3.7×10^{-2}
ASZ-2	-0.668	1.46×10^{-8}	1.46×10^{-8}	4.6×10^{5}	4.75×10^{-6}

From the results (Table 6), due to laser surface alloying, there was an increase in the value of the corrosion potential E_{corr} from -1.036 V of the AA1200 alloy to -0.668 V of the alloyed sample. Equally, the polarization resistance increased with lower corrosion rate for the laser surface alloyed sample. The micrograph on Figure 4 (a) reveals the needle-like platelets structures that are present in the laser alloyed matrix and XRD spectrum (Figure 6 (b)) reveals the kind of phases that are formed during the alloying, which are responsible for the increased corrosion resistance. The enhanced surface properties obtained can be attributed to these microstructural/phases changes occurring in the developed alloys. The phases that are formed include; α-Al, Al_3Co and Al_3Zr; the Al_3Zr phase formed is more dominant on the microstructure of the alloyed layer.

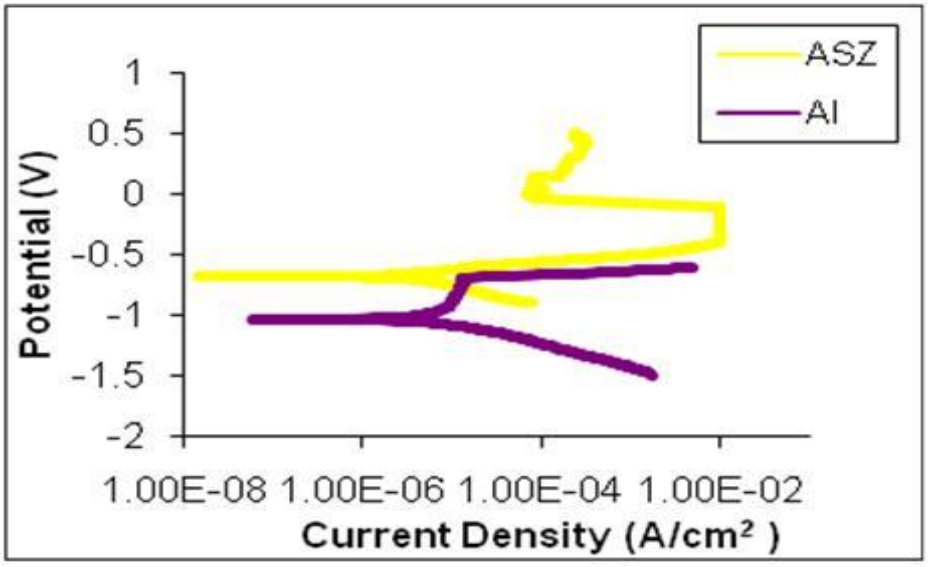

Figure 9. Linear polarization curves of AA1200 and Al-Zr-Stellite-6 sample

The comparison of Al and ASZ-2 samples showed that the corrosion current (i_{corr}) and corrosion density (j_{corr}) were reduced by two orders of magnitude (see Figure 9). A four order magnitude decrease in corrosion rate was observed for laser alloyed sample indicated by a 4.75 x 10^{-6} mm/yr and 3.7 x 10^{-2} mm/yr for the alloyed and as-received samples respectively. The reaction between the substrate and the alloying elements leading to newly formed microstructure/phases are responsible for the increase in corrosion resistance, homogeneous dispersion of the alloying materials in the melt pool also played a very crucial role in achieving better corrosion performance. Since aluminium is very active the addition of alloying elements reduces its activity thereby increasing its corrosion resistance. The following reactions occur during the process of corrosion testing when untreated Al was immersed in the chloride solution:

$$Al \rightarrow Al^{3+} + 3e^{-}$$
$$O_2 + 2H_2O + 4e^{-} \rightarrow 4OH^{-}$$
$$Al + 3OH^{-} \rightarrow Al(OH)_3$$

The aluminium metal was oxidised to its trivalent cationic state (Al^{3+}) from its zero oxidation state. The reduction in oxygen content is the result after the process of oxidation. The corrosion of aluminium led to the formation of insoluble aluminium hydroxide ($Al(OH)_3$) and subsequently the formation of basic hydroxychloride aluminium salt $Al(OH)_3Cl$ when reaction with chloride ions occurs. The halide ion penetrates the oxide film and corrosion reaction propagates. The oxide film on the surface of the Al is then thinned as a result of disintegration of Al.

However, after laser surface alloying, the corrosion behaviour of Al became much better. Visual examination of the surfaces of the samples tested revealed that the pure Al suffered deep corrosion attack while for the alloyed sample the corrosion attcak was very much reduced. At the

alloyed zone, corrosion reactions were hindered by the presence of thin oxide films and hence the sample exhibited good corrosion resistance in NaCl solution. The polarization resistance of the alloyed sample is also commendable; a two order magnitude increase was accomplished after surface alloying of Al.

Laser surface alloying process is not however without limitations and it should be noted that corrosion performance is very sensitive to any form of surface inhomogeneity. Microstructural inhomogeinety as a result of solidification behaviour and the difference in mixing of the alloying elements and substrate does exist during laser processing. Limitations such as pores, cracks and holes in the alloyed zone cannot be completely eliminated. Which therefore means that the corrosion performance of the alloyed sample would bave been much better than the actual values recorded. According to [12], limitations of the LSA process can be greatly minimized by proper selection of optimal process parameters that will yield perfectly homogeneous microstructure and hence high corrosion resistance of alloyed samples.

4. CONCLUSIONS

- There was an increase in hardness of the laser alloyed sample and the increase was 5-9 times that of the aluminium substrate
- The lower the scanning speed the higher the hardness and conversely high scanning speed showed reduced hardness.
- ASZ-2 showed high resistance to wear rate compared to other samples. The increase is due to the formation of new phases such as Al_3Co and Al_3Zr that were observed.
- ASZ-2 also showed an increase in corrosion resistance over other samples when compared to Al substrate. The increase in corrosion resistance was due to the formation of protective oxide films.
- Therefore, for improved surface properties (hardness, wear and corrosion resistances, the optimized laser processing parameters when stellite-6 and zirconium powders are used as reinforcement materials for LSA of aluminium substrate is laser power 4 kW, scan speed 1.2 m/min and powder flow rate 3 g/min; for improved hardness, wear and corrosion resistances properties.

ACKNOWLEDGEMENTS
This material is based upon work supported financially by the National Research Foundation. The National Laser Centre, CSIR, Pretoria is appreciated for laser facility. PISA is gratefully acknowledged for funding the students: TG Rambau and T Mathebula. Ms. Maritha Theron is appreciated for being an excellent mentor of the above-named students.

References

1. K. G. Watkins, M.A. McMohon and W. M. Steen, *Mater. Sci. Eng.*, A231 (1997) 55-61.
2. Y. Pei and J.Th.M.D Hosson, HYPERLINK "http://www.edax.com" www.edax.com ,(2002).

3. N. Ravi, D. Sastikumar, N. Subramanian, A. K. Nath and V. Masilamani, *Materials and Manufacturing Processes,* 15(3) (2000) 395-404.
4. Y. Chuang, S. Lee and H. Lin, *Materials Transactions*, 47(1) (2006) 106-111.
5. L.A.B Mabhali, S. L. Pityana and N. Sacks, *Molecular Crystals and Liquid Crystals*, 555 (1) (2012) 138-148.
6. P. Kadolkar and N. B, Dahotre, *Applied Surface Science*, 199 (2002) 222-233.
7. Y. Fu, A. W. Batchelor and N. L. Loh, *Wear*, 218(1998a) 250-260.
8. Y. Fu, A. W. Batchelor, Y. Gu, K. A. Khor and H. Xing, *Surface and Coatings Technology*, 99 (1998b) 287-294.
9. H.C. Man, S. Zhang T. M. Yue and F. T. Cheng, *Surface and Coatings Technology*, 148 (2001) 136-142.
10. A. P. I. Popoola, S. L. Pityana and O. M. Popoola, *International Journal of Electrochemical Science*, 6 (2011a) 5038-5051.
11. A.P.I. Popoola, S. L. Pityana and O. M. Popoola, *The Journal of South African Institute of Mining and Metallurgy*, (2011b) 345-353.
12. A. P. I. Popoola, S. L. Pityana and O. M. Popoola, *Journal of Laser Applications*, (2011c) 032003-1-9.
13. C. Chen, M. Zhang, Y. Su, S. Zhang, Q. Chang and X. Chen, *Project Grant Report*, 978-1-4244-7739-5/10/$26.00 2010 IEEE, (2010)
14. A. Almeida and R. Vilar, *Rev. Metal. Madrid*, 34(2) (1998) 114-119.
15. N. B. Dahotre, *ASM International*, 1 (1998).
16. S Nath, S. Pityana and J. D, Majumdar, *Surface & Coatings Technology*, (2012) 3333–3341.
17. H. Man, S. Zhang and F. T. Cheng, *Material letters*, (2007) 4058–4061.
18. C. Yao-Chih, L. Shih-Chin and L. Hsin-Chih, *The Japan Institute of Metals*, 47(4) (2006) 1140-1144.
19. M. H. Staina, M. Cruz and N. B. Dahotre, *Elsevier*, 1459-1468, (2001).